The Synthesis, Structure, and Bonding of Sc_8Te_3 and Y_8Te_3. Cooperative Matrix and Bonding Effects in the Solid State

Paul A. Maggard and John D. Corbett*

Department of Chemistry, Iowa State University, Ames, Iowa 50011

Received August 29, 1997

Sc_8Te_3 and Y_8Te_3 have been prepared by high-temperature solid-state techniques. The structures of both were determined from single-crystal and powder X-ray diffraction methods to be monoclinic, *C*2/*m* (No. 12) with $Z = 8$. Accurate lattice constants from Guinier powder film techniques at 23 °C for Sc_8Te_3 are $a = 28.842(7)$ Å, $b = 3.8517(6)$ Å, $c = 22.352$ (5) Å, $\beta = 122.51(2)°$; those for Y_8Te_3 are $a = 31.153(7)$ Å, $b = 4.0703(4)$ Å, $c = 24.375(5)$ Å, $\beta = 122.80(2)°$. The layered structure of the title compounds consists of a complex network of chains of trans-edge-sharing metal octahedra condensed into two types of corrugated sheets that are separated by tellurium. In terms of metal−metal bonding (as judged by overlap populations), the isotypic Ti_8S_3 and Ti_8Se_3 are more 3D in aggregation, while these scandium and yttrium tellurides are 2D. This difference in dimensionality is attributed to the cooperative effects of increased anion size and decreased valence electron concentration. This is described in detail for Sc_8Te_3. Contrasting paramagnetic properties are reported for the two, Pauli-like for Y_8Te_3 and temperature-dependent for Sc_8Te_3, in parallel with the behaviors of the parent metals.

Introduction

The study of reduced chalcogenides of the early transition metals has led to a great variety of new chemistry and to a broader understanding of the bonding in solids. Examples of reduced group 4 chalcogenides include, but are not limited to, Ti_8Z_3[1,2] and Ti_2Z,[3,4] (Z = S,Se), $Ti_{11}Se_4$,[5] Ti_9Se_2,[6] Hf_2Te,[7] Hf_3Te_2,[8] Hf_2Se_3,[9] and Zr_3Te.[10] While the metal-rich chalcogenides of groups 4 and 5 transition metals have been heavily explored, those of the group 3 transition elements are almost unknown, the only example being the recently discovered Sc_2Te with a complex chain structure for scandium.[11] Examination of the literature for the Sc−Te and Y−Te binary systems reveals no investigations into the metal-rich parts of either, and the most reduced compounds reported in both systems are R_2Te_3 and RTe (R = Sc, Y).[12,13] This paper describes the first metal-rich yttrium chalcogenide, Y_8Te_3, and the isotypic Sc_8Te_3.

To a chemist, "understanding" a structure usually means justifying its existence and stability. For reduced chalcogenides of the early transition metals, this may mean only a conclusion that the distances and apparent bonding in the structure are "reasonable". The problem is how to justify, or understand, the relative stability of one unremarkable phase in a binary system that has a few electrons holding together a metal fragment with little to no discernible preference for electron counts or directional bonding. For reduced chalcogenides, innumerable structures may seem reasonable, but there is no delineation between an imaginary and an actual structure. Articles have provided theories justifying the existence of some particular reduced chalcogenide relative to known structural alternatives and the elements. Recently, the valence electron concentration together with the cohesive energy of the metal was used to rationalize the existence and structure type of Hf_2Te (Nb_2Se type).[7] Alternatively, the stabilities of Ti_2S and Ti_8S_3 were attributed to the enhanced efficiency of both metal−metal and nonmetal−metal bonding in each compared with those in the pure metal and TiS.[14]

Clearly, atom sizes, valence electron concentrations, and the metal-to-nonmetal proportions play key roles in the determination of structure features and types. The structural features seen in transition-metal-rich chalcogenides are predominantly condensed body-centered cubes or distorted metal octahedra. With the discovery of more reduced chalcogenides of the earliest transition metals, new insights into stability may be gained about the interplay of the above three variables and how they influence the structural features seen in more electron-rich systems, Ti_8S_3 and Ti_8Se_3 in particular. No thorough analysis of the structure and bonding features in these titanium compounds has appeared, however. Some analysis of "where the electrons are" and of the interplay of matrix and bonding effects may be found in the results of extended Hückel calculations. The new Sc_8Te_3 and Y_8Te_3 are significant in that they represent the electron-poorest, yet among the most metal-rich chalcogenides of the transition metals reported to date.

(1) Owens, J. P.; Franzen, H. F. *Acta Crystallogr.* **1974**, *B30*, 427.
(2) Weirich, T. E.; Pöttgen, R.; Simon, A. *Z. Kristallogr.* **1996**, *211*, 929.
(3) Owens, J. P.; Conard, B. R.; Franzen, H. F. *Acta Crystallogr.* **1967**, *23*, 77.
(4) Weirich, T. E.; Pöttgen, R.; Simon, A. *Z. Kristallogr.* **1996**, *211*, 928.
(5) Weirich, T. E.; Ramlau, R.; Simon, A.; Hovmöller, S.; Zou, X. *Nature* **1996**, *382*, 144.
(6) Weirich, T. E.; Simon, A.; Pöttgen, R. *Z. Anorg. Allg. Chem.* **1996**, *622*, 630.
(7) Harbrecht, B.; Conrad, M.; Degen, T.; Herbertz, R. *J. Alloys Compd.* **1997**, *255*, 178.
(8) Abdon, R. L.; Hughbanks, T. *Angew. Chem., Int. Ed. Engl.* **1994**, *33*, 2414.
(9) Schewe-Miller, I. M.; Young, Y. G. *J. Alloys Compd.* **1994**, *216*, 113.
(10) Harbrecht, B.; Leersch, R. *J. Alloys Compd.* **1996**, *238*, 13.
(11) Maggard, P. M.; Corbett, J. D. *Angew. Chem., Int. Ed. Engl.* **1997**, *36*, 1974.
(12) (a) Men'kov, A. A.; Komissarova, L. N.; Simonav, Ju. P. *Dokl. Akad. Nauk. SSSR* **1961**, *141*, 364. (b) White, J. G.; Dismukes, J. P. *Inorg. Chem.* **1965**, *4*, 1760.
(13) Dismukes, J. P.; White, J. G. *Inorg. Chem.* **1965**, *4*, 970.
(14) Franzen, H. F. *Proc. 50th Anniv. Conf. Korean Chem. Soc.* **1996**, 635.

S0020-1669(97)01107-5 CCC: $15.00
Published on Web 02/04/1998

Table 1. Comparison of Lattice Parameters (Å, deg) and Cell Volumes (Å^3) for Known M_8Ch_3 Phases (Ch = S, Se, Te)

compound	*a*	*b*	*c*	*β*	*V*
Ti_8S_3[a]	25.13(1)	3.327(2)	19.36(2)	123.1(5)	1356(7)
Ti_8Se_3[b]	25.562(4)	3.4411(5)	19.701(6)	122.25(1)	1466(1)
Sc_8Te_3[c]	28.842(7)	3.8517(6)	22.352(5)	122.51(2)	2094(2)
Y_8Te_3[c]	31.153(7)	4.0703(4)	24.375(5)	122.80(2)	2598(2)

[a] Reference l, converted to the same setting as for Sc_8Te_3. [b] Reference 2. [c] For λ = 1.540 562 Å; 23 °C, space group *C*2/*m*.

Experimental Section

Synthesis. All materials were handled in He-filled or N_2-filled gloveboxes to reduce contamination by "adventitious" impurities. The syntheses of both Sc_8Te_3 and Y_8Te_3 began with the preparation of the corresponding Sc_2Te_3 and Y_2Te_3 phases (NaCl-type with disordered cation vacancies). The elements were used as received (Sc turnings, 99.7%, Aldrich; Y sheet, 99.8%, Alfa; Te powder, 99.99%, Aldrich) and were loaded in a 2:3 stoichiometry into a fused silica container. The fused silica container was evacuated, sealed off, and heated to 450 °C for 12 h and then to 900 °C for 72 h. The sample was allowed to cool radiatively to room temperature. Guinier film data confirmed the products were the R_2Te_3, NaCl-type phases. Appropriate amounts of these and scandium or yttrium metal to give the 8:3 stoichiometry were then pelletized inside a He-filled glovebox with the aid of a hydraulic press. The resulting pellets were arc-melted for 20 s per side with a current of 70 amps. Guinier patterns of the products at this point revealed a mixture of Sc_9Te_2[15] and Sc_2Te for the scandium reaction and a blurred pattern similar to that of Y_8Te_3 for the yttrium reaction. Each sample was then sealed inside tantalum tubing, annealed at 1150 °C for 72 h, and allowed to radiatively cool. It should be noted that annealing temperatures 10−20 °C still higher resulted in reaction of the scandium products with the tantalum and in subsequent failure of the tubing. After annealing, Guinier powder diffraction film data showed that both Sc_8Te_3 and Y_8Te_3 had been obtained in apparently quantitative yields (single phase).

Powder X-ray Diffraction. The powder diffraction patterns of Sc_8Te_3 and Y_8Te_3 were obtained with the aid of an Enraf-Nonius Guinier powder camera and monochromatic Cu Kα_1 radiation. The samples were crushed into powder form, mixed with standard silicon (NIST), and placed between two strips of Scotch-brand tape on a frame for mounting on the camera rotation motor. Lattice parameters were obtained by least squares from 35 measured and indexed lines per sample. The lattice parameters are given in Table 1 along with those for the two titanium analogues for comparison.

Single-Crystal Diffraction. Several black, irregularly shaped crystals were obtained from both the scandium and yttrium reactions. All crystals were mounted inside 0.3 mm i.d. glass capillaries that were sealed off and mounted on metal pins. Their crystal quality was checked by means of Laue photographs, and the best crystal from each group selected. A data set for the Sc_8Te_3 phase was collected on a CAD4 diffractometer (Mo Kα_1 radiation) at room temperature. Twenty-five centered reflections gathered from a random search were used to determine provisional lattice constants and the crystal system. Half a sphere of data was collected (h, ±k, ±l), and these were subsequently corrected for Lorentz and polarization effects. The data were further corrected for absorption with the aid of two averaged ψ scans. Of 4310 measured reflections ($2\theta \leq 50°$), 2233 had $I > 3\sigma(I)$, and 1356 of these were unique. Extinction conditions suggested the possible space groups *C*2, *Cm*, and *C*2/*m*. Because the intensity statistics indicated a centrosymmetric space group, the structure was solved by direct methods (SHELXS[16]) and refined with the package TEXSAN in *C*2/*m*.[17] Subsequent refinements in the acentric space groups did not yield lower residuals or improved parameters. After isotropic refinement, the data were better corrected for absorption with respect to the third dimension of the crystal by means of DIFABS[18] and then averaged with R_{ave} = 9.0%. The final refinement converged at *R(F)*/R_w = 3.7/3.7% for the loaded composition Sc_8Te_3. Selected crystallographic data, atomic positions, and isotropic-equivalent temperature factors are given in Tables 2 and 3. Additional data collection and refinement parameters, the anisotropic displacement parameters, and a complete distance list are in the Supporting Information. These, as well as the F_o/F_c listing, are also available from J.D.C.

Table 2. Selected Crystal and Refinement Data for Sc_8Te_3[a]

fw	742.45
space group, *Z*	*C*2/*m* (No. 12), 8
d_{calc}, g cm^{-3}	4.710
μ(Mo Kα), cm^{-1}	130.4
rel transm coeff range	0.832−1.00
R, R_w,[b] %	3.7, 3.7

[a] Lattice dimensions in Table 1. [b] $R = \sum||F_o| - |F_c||/\sum|F_o|$; $R_w = [\sum w(|F_o| - |F_c|)^2/\sum w(F_o)^2]^{1/2}$; $w = \sigma_F^{-2}$.

Table 3. Positional and Isotropic Thermal Parameters for Sc_8Te_3[a]

atom	*x*	*z*	B_{eq} (Å^2)[b]
Te1	0.74108(6)	0.2799(1)	0.76(5)
Te2	0.89524(6)	0.3142(1)	0.72(6)
Te3	0.05620(6)	0.8265(1)	0.80(6)
Te4	0.42614(6)	0.8074(1)	0.72(6)
Te5	0.86962(6)	0.9628(1)	0.85(6)
Te6	0.86855(6)	0.4690(1)	0.77(6)
Sc1	0.4081(1)	0.5890(2)	0.9(2)
Sc2	0.2773(2)	0.3979(2)	0.8(2)
Sc3	0.3029(2)	0.2457(2)	1.0(2)
Sc4	0.4262(2)	0.4318(3)	1.2(2)
Sc5	0.4371(2)	0.9468(2)	0.7(2)
Sc6	0.0087(2)	0.9131(2)	0.9(2)
Sc7	0.9383(2)	0.7147(2)	1.0(2)
Sc8	0.7987(2)	0.5304(3)	1.2(2)
Sc9	0.7116(2)	0.1334(2)	0.9(2)
Sc10	0.6712(2)	0.3443(2)	1.0(2)
Sc11	0.6340(2)	0.9376(2)	0.7(2)
Sc12	0.4615(2)	0.2859(2)	0.7(2)
Sc13	0.8329(2)	0.1532(3)	1.3(2)
Sc14	0.1507(2)	0.1911(2)	0.5(1)
Sc15	0.2398(2)	0.0431(3)	1.7(2)
Sc16	0.9882(2)	0.5681(2)	1.2(2)

[a] All atoms in position 4*i*, y = 0. [b] $B_{eq} = (8\pi^2/3)\sum_i\sum_j U_{ij}a_i^*a_j^*\vec{a}_i\vec{a}_j$.

The diffracting powers of the scandium crystals were in all cases much better than for the Y_8Te_3 crystals. A data set collected on the best diffractor among the yttrium crystals gave only ~20% observed reflections. The structure could be refined isotropically to R_w < 8% as isostructural with Sc_8Te_3, but the number of observed data were generally insufficient and these were very weak. Nonetheless, the atomic positions found and the observed X-ray powder diagrams made it clear that Y_8Te_3 has the same structure as Sc_8Te_3.

The unit cell choice for Table 3 needs to be made clear. We have retained the origin as reported for the original Ti_8S_3[1] (the center of the Sc16−Sc16 bond) but have transformed the cell to give the preferred cell with the smaller (obtuse) β angle. The later report on Ti_8Se_3[2] has the same cell but with the origin displaced from ours by *c*/2.

Properties. Powdered samples of ~50 mg of Sc_8Te_3 and Y_8Te_3 were each loaded inside a He-filled glovebox so that they were sandwiched between two glass rods inside a 3 mm i.d. fused silica tube. Magnetizations for the samples were measured from 6 to 300 K in a field of 3 T with the aid of a Quantum Design MPMS SQUID magnetometer. The data were corrected for diamagnetism of both the sample holder and atom cores. Resistivities of powdered, sized samples of ~50 mg of Sc_8Te_3 and Y_8Te_3 diluted with Al_2O_3 were each measured with a "Q" apparatus between 100 and 300 K.

(15) Maggard, P.; Corbett, J. D. Unpublished research (Sc_9Te_2).
(16) Sheldrick, M. *SHELXS-86*; Universität Göttingen: Germany, 1986.
(17) *TEXSAN*, version 6.0; Molecular Structure Corp.: The Woodlands, TX, 1990.
(18) Walker, N.; Stuart, D. *Acta Crystallogr., Sect. A.* **1983**, *39*, 158.

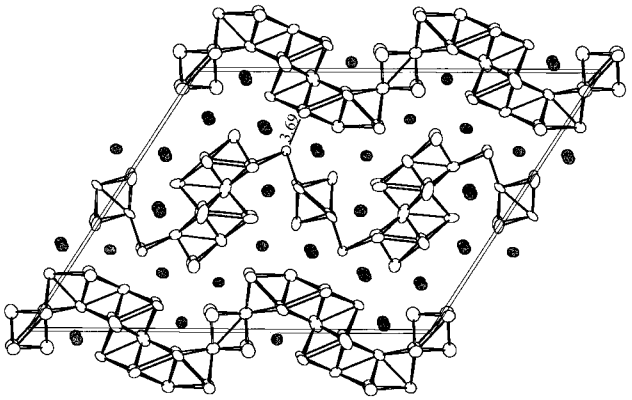

Figure 1. Near-[010] projection of the unit cell of Sc_8Te_3 (99.9% probability thermal ellipsoids) with bonds drawn for $d(Sc-Sc) \leq 3.50$ Å. The shortest intersheet distance, Sc10−Sc14, is marked. Dark atoms are tellurium; light atoms, scandium.

Band Calculations. Extended Hückel calculations were carried out within the tight-binding approximation[19] for the full structure of Sc_8Te_3 at 32K points spread out over the irreducible wedge. H_{ii} parameters employed were the same as the charge-iterated values obtained previously for Sc_2Te[11] (in eV). For Sc: 4s, −6.75; 4p, −3.38; 3d, −6.12. For Te: 6s, −21.20; 6p, −12.00.

Results and Discussion

Structural Description. A near-[010] section of the Sc_8Te_3 structure down the short (3.85 Å) *b* axis is given in Figure 1. Evident are two separate and independent corrugated chains of scandium atoms along $\vec{a}$ that are separated by tellurium atoms along $\vec{c}$. The scandium atoms are further bonded down the short projection axis into layers (not shown). The shortest distance between the corrugated sheets is the 3.69 Å marked for Sc10−Sc14, which will be shown to be a nonbonding interaction. The Sc−Sc distances within these chains vary semicontinuously from 3.00 to 3.48 Å, as shown in Table 4 and marked separately in Figure 2. There are no distinctive breaks in this range, and the next larger value, 3.67 Å, is a fairly special interaction. This length trend is quite similar to that observed in Sc_2Te. The scandium−scandium distance limit in drawing bonds in the figures has been set at 3.5 Å, in correspondence with the analysis of Sc_2Te and as likewise justified later in terms of overlap populations. The observed (12-bonded) and calculated single-bond metallic distances for the pure metal are 3.24 and 2.88 Å,[20] so the observations for Sc_8Te_3 pertain to relatively electron-poor delocalized bonding.

Both corrugated sheets contain structural building blocks that are grossly similar to those in the isostructural Ti_8S_3 and Ti_8Se_3. The structure of Ti_8S_3 was described in terms of condensed body-centered cubes,[1] while the structural features in Ti_8Se_3 were described as condensed, distorted octahedra.[2] Preference will be given to the condensed, distorted octahedra description here, with some mention of the body-centered cubic features when appropriate. In the less condensed chain or sheet, Figure 2A, two main scandium units are evident, an infinite trans-edge-sharing chain of single octahedra (Sc5 and Sc6) and four infinite trans-edge-sharing chains of octahedra condensed through sharing of six side edges (not faces). (Such condensation, but only of a pair of chains, was first observed in Sc_7Cl_{10}.[21]) The quadruple chain is called the Z unit from here on (Sc3, Sc9, Sc11, Sc13, Sc15). The Z unit is also clearly two interpenetrating body-centered cubes centered by Sc15, e.g., Sc9, 11, 15, 13. The single edge-sharing octahedral chain has the shortest distance among the shared edges (Sc5−Sc5, 3.09 Å) and longer apex distances for the nonshared edges (Sc5−Sc6, 3.20 Å, 3.27 Å). The vertex−vertex distance, Sc6−Sc6, is correspondingly large. The Z unit likewise has the shortest distances among the shared edges of different octahedral chains (Sc15−Sc15, 3.00 Å; Sc13−Sc15, 3.14 Å) and longer distances among the outside (nonshared) and inside trans-edges of the chains (3.14−3.43 Å). It is not by chance that the shorter scandium distances in the sheet are those furthest from the tellurium positions. The Z units and the single octahedral chains are connected via the lone Sc14 atoms (Sc5−Sc14, 3.35 Å; Sc9−Sc14, 3.30 Å) to generate the sheet, or puckered layer, but these are very weak bonds (below).

The repeating unit in the other more condensed corrugated sheet is shown in Figure 2B. The same Z unit can be discerned in the middle of the figure (Sc1, 2, 7, 8, 10). But this unit is now further condensed on both ends through two fairly short edges (Sc1−Sc7, 3.12 Å) to strings of three octahedral chains that share vertexes internally. This assembly, repeated down the *b* axis, generates the second puckered layer or sheet with more Sc−Sc bonding, shorter distances and, presumably, tighter bonding than the first one. Again, the shortest distances occur in the shared edges of different octahedral chains of higher connectivity (Sc8−Sc8, 3.06 Å; Sc8−Sc10, 3.11 Å; Sc1−Sc7, 3.12 Å), with the longer scandium distances around the periphery, as before (3.13−3.48 Å). The unique octahedral chain that does not share vertexes, only waist atoms (Sc4, 16 in Figure 2B), is more squashed and has a relatively shorter vertex−vertex distance (3.67 Å) and stronger bonding therewith (below). The sheet in Figure 2B also has more body-centered fragments, those centered by Sc8 and (distorted) Sc16. The characteristic body-centered cubic fragments are more pronounced in Sc_8Te_3 than in the electron-poorer Sc_2Te and are even more pronounced in most of the electron-richer, metal-rich chalcogenides of the group 4 and 5 metals.

It should be noted that the relative cell dimensions and various modes of condensation seen in Figure 2 mean there are a wide variety of distances and distortions from idealized condensed octahedra. These occur particularly because of the long $\vec{b}$ repeat in the waist of all of the octahedra (3.85 Å) relative to the imagined shared trans-edges near 3.30 Å. Thus the average scandium octahedron is also compressed along the vertex−vertex direction by about 0.4 Å relative to the ideal model. These differences are further compounded by the marked shortening of most of the side edges that are shared between octahedral chains. Notwithstanding, the octahedral units still remain the best overall descriptors for these structures.

All tellurium atoms in Sc_8Te_3 are surrounded by trigonal prisms of metal on which the rectangular faces are further capped one to three times by more scandium. The Sc−Te distances vary only from 2.91 to 3.01 Å. All Te−Te distances are ≥3.83 Å, and so Te−Te bonding is not a significant concern.

Although a good-quality data crystal could not be found for Y_8Te_3, it is clearly isostructural with Sc_8Te_3. The change in the metal causes a shift to larger lattice constants (Table 1) and therefore longer metal−metal distances, by 0.25−0.40 Å or to ∼10% greater than in Sc_8Te_3. The bonding trends and features in Sc_8Te_3 are equally valid for Y_8Te_3 save for one important feature, a changed size differentiation between R and Te in what can be called a matrix effect (below).

(19) (a) Hoffman, R. *J. Chem. Phys.* **1963**, *39*, 1397. (b) Whangbo, M.; Hoffman, R. *J. Am. Chem. Soc.* **1978**, *100*, 6093.
(20) Pauling, L. *The Nature of the Chemical Bond*; Cornell University Press: Ithaca, NY, 1960; p 400.
(21) Hwu, S.-J.; Corbett, J. D.; Poeppelmeier, K. F. *J. Solid State Chem.* **1985**, *57*, 43.

Table 4. Selected Pairwise Distances in Sc_8Te_3 Ordered According to Their Corresponding Overlap Populations

atom 1	atom 2	distance (Å)	overlap	atom 1	atom 2	distance (Å)	overlap
Sc15	Sc15	3.00(1)	0.343	Sc16	Sc16	3.456(9)	0.124
Sc5	Sc5	3.09(1)	0.334	Sc11	Sc15	3.425(6)	0.119
Sc8	Sc8	3.058(7)	0.316	Sc7	Sc10	3.308(5)	0.119
Sc8	Sc10	3.113(5)	0.316	Sc10	Sc10	3.8517(6)	0.119
Sc1	Sc7	3.119(4)	0.312	Sc13	Sc13	3.8517(6)	0.117
Sc13	Sc15	3.142(5)	0.297	Sc16	Sc16	3.8517(6)	0.114
Sc1	Sc12	3.265(5)	0.263	Sc8	Sc8	3.8517(6)	0.114
Sc9	Sc13	3.282(6)	0.220	Sc15	Sc15	3.8517(6)	0.111
Sc5	Sc6	3.195(5)	0.209	Sc2	Sc8	3.301(5)	0.106
Sc2	Sc8	3.339(6)	0.204	Sc1	Sc8	3.306(5)	0.100
Sc4	Sc16	3.130(5)	0.178	Sc12	Sc16	3.373(5)	0.099
Sc1	Sc10	3.334(6)	0.176	Sc7	Sc12	3.479(5)	0.093
Sc3	Sc9	3.138(5)	0.174	Sc7	Sc7	3.8517(6)	0.074
Sc11	Sc15	3.425(6)	0.171	Sc1	Sc1	3.8517(6)	0.069
Sc5	Sc6	3.272(5)	0.155	Sc3	Sc15	3.869(8)	0.064
Sc4	Sc16	3.214(5)	0.149	Sc6	Sc6	3.8517(6)	0.060
Sc9	Sc15	3.196(6)	0.149	Sc13	Sc15	3.709(8)	0.059
Sc3	Sc13	3.265(5)	0.146	Sc9	Sc9	3.8517(6)	0.056
Sc4	Sc4	3.672(9)	0.141	Sc5	Sc5	3.8517(6)	0.055
Sc1	Sc16	3.230(5)	0.140	Sc9	Sc14	3.299(5)	0.048
Sc2	Sc10	3.251(5)	0.139	Sc8	Sc10	3.794(7)	0.043
Sc11	Sc13	3.289(5)	0.129	Sc5	Sc14	3.352(5)	0.040

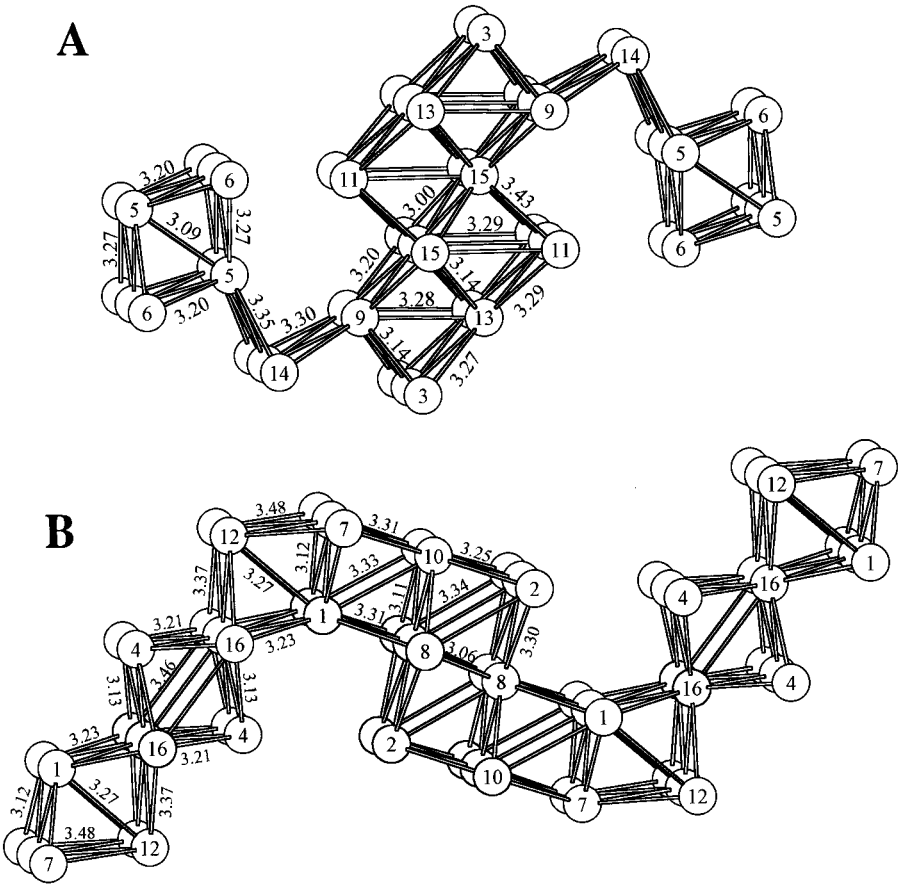

Figure 2. (A) More open corrugated sheet in Sc_8Te_3 with bond distances marked. The sheet is infinite along the projection axis. Two-fold axes pass through the centers of the Sc5−Sc5 and Sc15−Sc15 bonds. (B) More condensed corrugated sheets in Sc_8Te_3. Two-fold axes pass through the centers of the Sc8−Sc8 and Sc16−Sc16 bonds.

Calculations. Figure 3 shows the total DOS (densities of states) for Sc_8Te_3. The Fermi level (solid line) lies in a valley between two smallish peaks in a region that is dominated by scandium d orbital contributions; hence the solid is metallic. The dashed line is the projection of tellurium contributions, which are significant in this range only in the upper energy levels, well above E_F. Figure 4 shows the COOP (crystal orbital overlap population) curve for the total Sc−Sc bonding in Sc_8Te_3. As in Sc_2Te, many metal−metal bonding states above E_F remain unoccupied. Two small peaks in the DOS around the Fermi level are both Sc−Sc bonding while the largest peak above them (−5.9 eV) is a mixture of nonbonding and antibonding states. As seen before in Sc_2Te, the interesting array of small peaks in the DOS at −7.0 eV and below arise from specific Sc−Sc interactions at shorter and shorter distances.

Such a complex structure as this provides a wide variety of distances and, presumably, bond strengths that need to be sorted out. Distances alone, although often taken to somehow vary

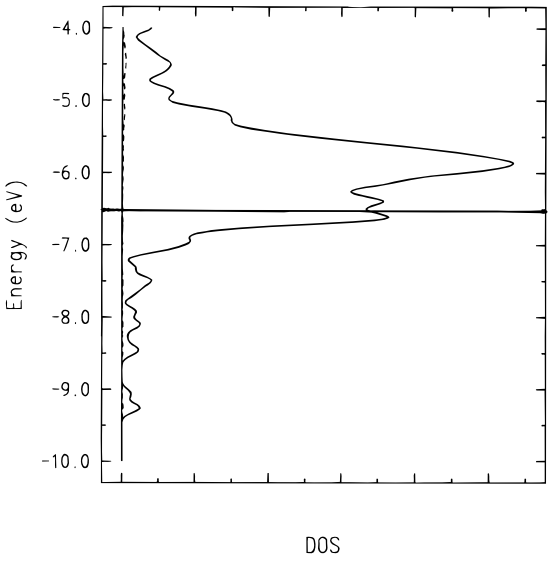

Figure 3. Total densities of states (DOS) for Sc_8Te_3. The dashed line is the projection of the tellurium contributions.

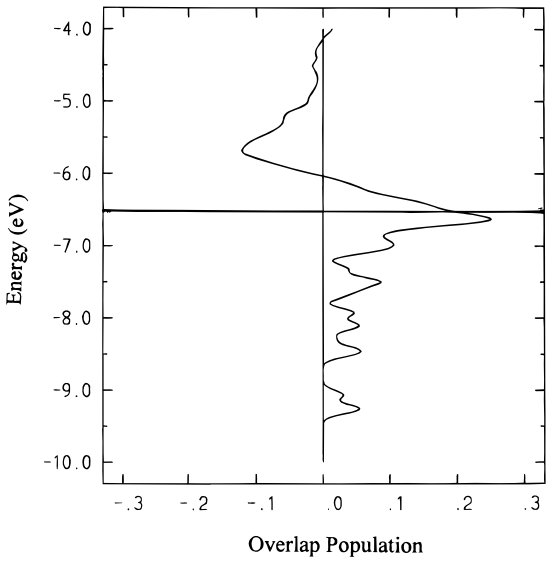

Figure 4. Total Sc−Sc crystal orbital overlap population out to 3.8 Å.

inversely with the strength of the interactions, can be very misleading when these are determined largely or solely by matrix effects, that is, by just the contact sizes of the packed units. Examples can be clearly seen in Sc_2Te.[11] The interlayer (sheet) distances in the present structure, Sc10−Sc14 for example (3.69 Å, Figure 1), are certainly of this character as these are established principally by the size of tellurium, with vanishingly small evidence of bonding according to the overlap population sum (OP) up to E_F for each atom pair.

For these purposes, pairwise overlap populations are used in Table 4 as the basis for ordering the listed distances. As expected, the overlap populations generally correlate with the bond distances, but there are some significant deviations that reflect important bonding details. The six largest overlap populations are associated by and large with the six shortest distances. One is the shared Sc5−Sc5 edge in the nearly isolated octahedral chain, but the other five short distances and large overlap populations pertain to the shared interior edges between octahedral chains (Sc pairs 15−15, 8−8, 8−10, 1−7, 13−15) at 3.00−3.14 Å. As found with Sc_2Te, the theme is that electrons are concentrated within the condensed units and

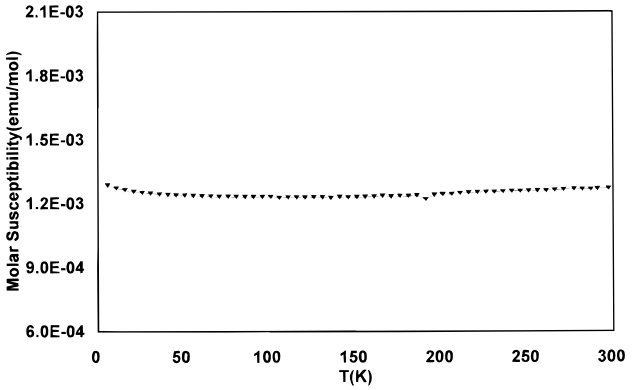

Figure 5. Molar magnetic susceptibility of Y_8Te_3 as a function of temperature (K).

thereby give rise to higher overlap populations. (Use of these pairwise measures may still leave delocalized (multicenter) bonding underappreciated.) In contrast, the outer regions of these, where scandium has fewer like and more tellurium neighbors, have low overlap populations relative to the distances. In the first category are the longer shared-waist distances that have relatively high populations, namely atom pairs 1−10, 1−12, 2−8, 9−13, and 11−15 at 3.26−3.34 Å with OP values of 0.171 to 0.263. In contrast, the pair populations for the distances around the outside of the condensed units have low OP values relative to the distances, viz., 3−9, 3−13, 9−15, and 11−13 in Figure 2A and 1−16, 2−8, 2−10, 4−16 (×2), 7−10, and 12−16 in Figure 2B. Unshared trans vertexes in octahedra give rise to relatively high OP's and short bonds, i.e., about Sc6 in the lone single chain (2A) and for the trans Sc4−Sc4 pair (2B), where a long 3.67 Å separation in the latter has an OP value of 0.141. The last is the only contradiction of the 3.50 Å upper limit used for bonds in the figures. The single octahedral chain of Sc5 and Sc6 is relatively isolated since the overlap populations for the "bonds" to the bridging Sc14 are only 0.04 and 0.05. Of course, significant bonding along *b*, the 3.85 Å projection axis, is expected for what is described as a 2D corrugated sheet structure, and 10 of the 16 Sc_i−Sc_i overlap populations are large enough to appear in Table 4.

Evidence that electrons are preferentially delocalized within the aggregated cluster sheets while being removed from the outlying Sc atoms with more Te neighbors is a recurrent theme. The shortest interlayer distance, 3.69 Å for Sc10−Sc14 in Figure 1, has an overlap population of only ca. 5×10^{-4}! Interactions between filled, low-lying tellurium orbitals with higher lying orbitals on nearest neighbor scandium atoms have the effect of pushing the latter even higher in energy, so that they do not interact and bond as well with interior scandium atoms. Drawing bonds in this structure based only on distances is misleading. In a relatively electron-poor but metal-rich system, geometry, efficient packing, and stoichiometry dictate that some metal atoms must be packed close together even if there are no electrons for their bonding. Thus, scandium pairs such as 9−14 and 5−14 with small OP's are held together not by bonding electrons, but through common electrostatic and covalent interactions with their anionic tellurium neighbors. This is similar to the way in which lithium atoms in LiF are held close by surrounding fluorine atoms, and the zigzag scandium chain in Sc_2Te, by surrounding tellurium atoms. In other words, these group 3 chalcogenides all illustrate how matrix effects, dictated by simple geometry and efficient packing considerations, cooperate with the "electronics" or bonding within the solid to generate stable phases in a relatively electron-poor system. While the overlap populations should in the simplest cases

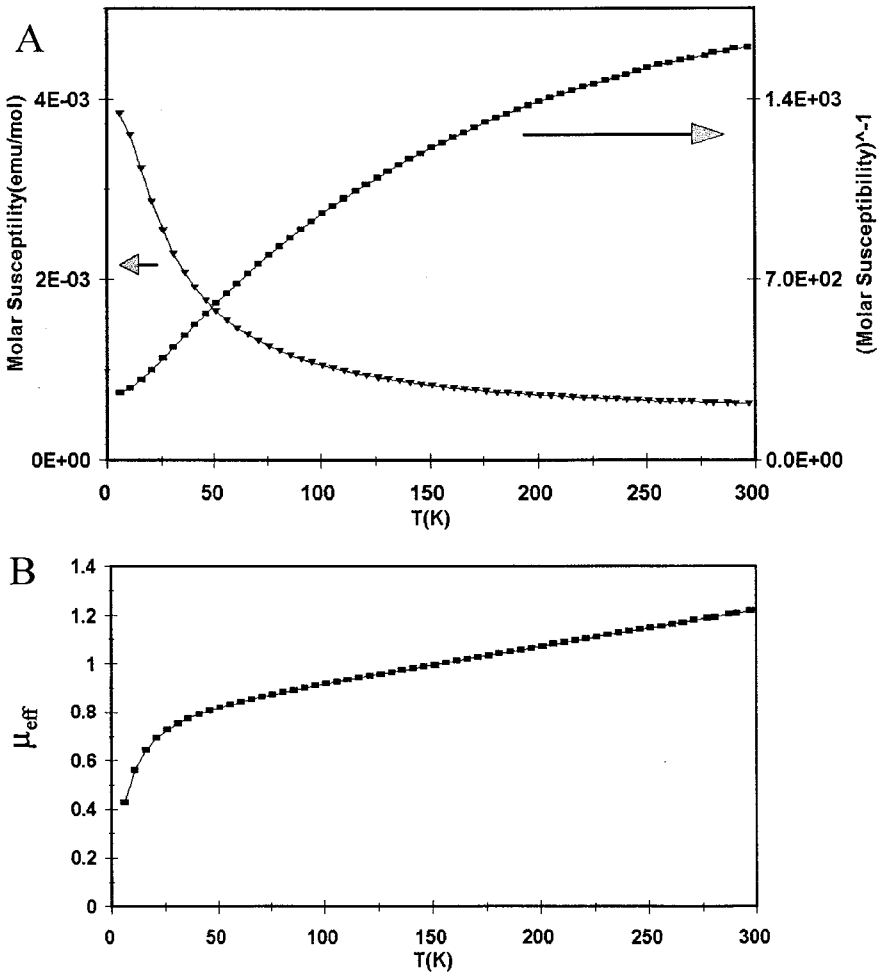

Figure 6. (A) Molar magnetic susceptibility of Sc_8Te_3 and its inverse as a function of temperature. (B) M μ_{eff} vs temperature for Sc_8Te_3.

correlate with distances (and Pauling bond orders), both the positions of the "bonds" relative to the metal aggregate and the number of anion neighbors have a considerable effect on the actual overlap between a particular pair of metal atoms. In Sc_8Te_3 and Sc_2Te, the scandium bonding is primarily within and between the trans-edge-sharing octahedra chains, while the outlying scandium atoms are held together more by a cooperative network of tellurium atoms.

Property Measurements. Because of the nature of the metal−metal bonding and the sizable densities of states at E_F from extended Hückel calculations, both Sc_8Te_3 and Y_8Te_3 are expected to be metallic and Pauli-paramagnetic. High-frequency measurements of resistivities of the polycrystalline R_8Te_3 phases over 100−300 K showed that both are metallic but are rather different. The resistivity of Sc_8Te_3 is ∼143 $\mu\Omega$ cm at 298 K, 2.5 times that of the metal,[22] with a temperature dependence of 0.16% K^{-1}, while that for Y_8Te_3 is ∼226 $\mu\Omega$ cm, 3.8 times that of the metal[22] and with a variation of 0.39% K^{-1}. Both reflect the higher anisotropy of the binary structure type. The magnetic differences are also sizable. Figure 5 shows that Y_8Te_3 exhibits a Pauli-like, temperature-independent paramagnetism of about 1.25×10^{-3} emu mol^{-1}, seven times that for pure yttrium metal, which is $\sim 1.8 \times 10^{-4}$ emu mol^{-1} and also temperature-independent.[23] The ratio of susceptibilities is roughly proportional to the 8:1 molar ratio of yttrium atoms in the two. Although nonmagnetic impurities in yttrium metal (such as oxygen or hydrogen) are reported to reduce the magnetic susceptibility,[23] the large structural change for Y_8Te_3 makes improbable its interpretation as essentially yttrium metal with tellurium as an impurity. The substantial rearrangement and changed bonding still appears to give about the same DOS at E_F judging from the susceptibility data and then perhaps a similar number of conduction electrons, but this is not reflected in the resistivity results, perhaps because of the higher anisotropy. In further contrast, Sc_8Te_3 exhibits a quite different and more complex paramagnetic behavior, Figure 6A, with an appreciable temperature dependence. The effective moment vs temperature is shown in Figure 6B. The data cannot be fit well by a simple nonlinear least-squares function that includes Curie−Weiss and van Vleck-like terms. Pure scandium metal over ∼70−300 K shows a smaller temperature dependence.[22] Although the earlier data have been described with a Curie−Weiss fit, $\mu_{eff} = 1.65\ \mu_B$, $\theta \sim -850$ K, this is not a realistic treatment. The 25% increase observed in the scandium metal susceptibility between 300 (2.95×10^{-4} emu mol^{-1}) and 75 K could well arise from a temperature dependence of the density of states at E_F and thence of the observed χ_P. In fact, band calculations for scandium show a large peak at E_F.[24] The situation with Sc_8Te_3 is clearly not so simple. The room-temperature value per scandium in Sc_8Te_3 is about one-fourth of that of the metal, and the temperature dependence, nearly five times greater. This may represent intermediate interactions

(22) Spedding, F. H.; Croat, J. J. *J. Chem. Phys.* **1973**, *58*, 5514.
(23) Spedding, F. H.; Croat, J. J. *J. Chem. Phys.* **1973**, *59*, 2451.
(24) (a) Theisen, C. M. Ph.D. Dissertation, Iowa State University, 1983. (b) Harmon, B. N. Private communication.

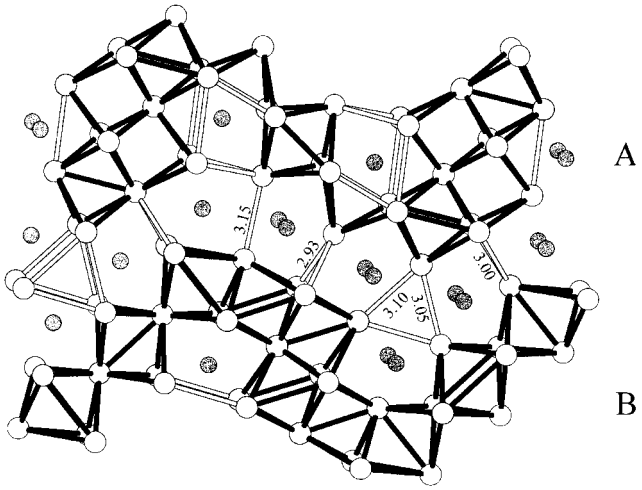

Figure 7. Near-[010] projection of the corrugated sheets in Ti_8S_3, with bonds drawn for d(Ti−Ti) < 3.20 Å. Dark bonds are comparable to those in the chains shown in Figure 2, while open bonds are additional interactions in this structure. The interlayer distances are marked. Dark atoms are sulfur; light atoms, titanium.

in which itinerant electrons gain small orbital contributions at particular cores.[25] With 16 unique Sc atoms in this structure, the possibilities are large, and the answer, probably complex.

Structural Comparisons. Although Sc_8Te_3 and Y_8Te_3 are isotypic with both Ti_8S_3 and Ti_8Se_3, and the four structures do share approximately the same atomic positions, there are many differences in these relatively complex arrangements. The metal−metal bonding within the group 3 chalcogenides occurs in essentially 2D corrugated sheets, as judged by both distances and overlap populations, but the titanium examples differ appreciably in the number of metal-based electrons and the size of the chalcogen spacers. Figure 7 shows an equivalent [010] view of the Ti_8S_3 structure, with the two corrugated sheets in this structure labeled A and B in analogy to Figure 2 and "bonds" drawn out to a limit of 3.2 Å. The intrasheet Ti−Ti distances in the sulfide range from 2.71 Å upward, with an average of 2.99 Å. To further aid the comparison, the metal−metal bonds marked in Figure 2 are shown as solid lines here, while any additional "bonds" are drawn as open connections. To make clear that the cutoff is not arbitrarily influencing the conclusion, an extended Hückel calculation and analysis on Ti_8S_3 was used to verify that 3.2 Å is a suitable limit for good bonding, as 3.5 Å is in Table 4.

Although the gross features of the corrugated sheets in Ti_8S_3 (Figure 7) are the same as with Sc_8Te_3, Figure 2, there are in detail two significant differences. First, reflecting the greater number of valence electrons is the generally greater condensation and increase in Ti−Ti bonding. Particularly chain A (Figure 7) is seen to contain many more "bonds" than does Figure 2A. The chain is internally more kinked and condensed, i.e., between the equivalent of atoms 5−9, 6−11, and 9−11 in Figure 2A. Two octahedral chains are also more squashed, and the trans-edge distances fall above the bond distance limit (11−15). The already more condensed chain B is less changed but has gained an additional 2−4 cross-link. Second and most important, distinctly more close contacts occur between the titanium sheets, from 3.15 Å down to a quite short 2.93 Å in what appears to be a more 3D metal−metal-bonded structure. The decreased anion size ensures more close contacts between the sheets, and the system appears to react cooperatively to the additional electrons from titanium with more bonding, especially interchain and in chain A. Thus, cooperative effects of decreased anion size, increased valence electron concentration, and the resulting shorter metal−metal distances stabilize this flexible structure. What seems to be enlightening is that the analogous Ti_8Te_3, Sc_8S_3, or Y_8S_3 with different size proportions have not been found, although this may result at least in part from inadequate efforts. The overall picture suggests there may be some kind of "magic" electron count needed to stabilize each structure, its features, or simply, the number of metal−metal bonds in a metal-rich compound. Electron count alone as a stability factor in metal-rich phases is perhaps less definite because of the delocalized bonding, while matrix effects are also a major factor.

Conclusions. The isotypic Sc_8Te_3 and Y_8Te_3 are significant in that they represent the electron-poorest, but yet the metal-richest chalcogenides reported for the early transition metals. Their chemistry relative to those of other early transition metal chalcogenides such as Ti_8Ch_3 provides insight regarding the bonding and existence of this novel structure type. Extended Hückel calculations help one to roughly "locate" the electrons in the solid and also allow one to assess the cooperative effects of anion size, cation positions, and valence electron concentration. Although Sc_8Te_3 and Y_8Te_3 exist in the same structure type as the sulfide and selenide of their electron-richer neighbor titanium, there are clear differences with the increased anion size, fewer elections, and larger metal distances in the former. This suggests that a particular but flexible electron count or valence electron concentration is necessary to stabilize what is also a flexible structure. Magnetic susceptibility measurements on both compounds show quite different results but are more similar to the differences in the pure metals themselves.

Acknowledgment. The authors thank Jerry Ostensen for the magnetic measurements and Len Thomas for upkeep of the single-crystal diffractometer. This work was supported by the National Science Foundation, Solid State Chemistry, with grant DMR-9510278 and was carried out in the facilities of the Ames Laboratory, U.S. Department of Energy.

Supporting Information Available: Tables of additional crystallographic and refinement parameters, anisotropic thermal parameters, and a complete listing of nearest-neighbor distances in Sc_8Te_3 (3 pages). Ordering instructions are given on any current masthead page.

IC971107Z

(25) Jiles, D. *Introduction of Magnetism and Magnetic Materials*, 2nd ed.; Chapman & Hall: London, 1998; p 316.